Bright Ring Lattice Generated by Nesting Spiral-Pinhole-Arrays Plate

Wenren Li
University of Electronic Science and Technology of China
Pusheng Liu (psliu@uestc.edu.cn)
University of Electronic Science and Technology of China
Yidong Liu
University of Electronic Science and Technology of China

Research Article

Keywords: bright ring lattice, orbital angular momentum

Posted Date: July 7th, 2021

DOI: https://doi.org/10.21203/rs.3.rs-671330/v1

Bright Ring Lattice Generated by Nesting Spiral-Pinhole-Arrays Plate

Wenren Li,[a] Pusheng Liu[a,*],Yidong Liu [a]

[a]*School of Physics, University of Electronic Science and Technology of China, Chengdu 611731, China*

Abstract: A nesting spiral-pinhole-arrays plate (NSP) is designed to produce bright ring lattice (BRL) formed by the superposition of two different orbital angular momentum (OAM) modes. The OAM modes of the BRL can be manipulated by the propagation distance and the spiral arrays of the NSP. We have studied the influences of rotating NSP on the BRL, and found that the rotational angle and direction of the BRL are not consistent with the results of the NSP.

Keywords：bright ring lattice; orbital angular momentum

1. Introduction

Optical vortex with a helical phase front of $exp(im\varphi)$ carry a well-defined orbital angular momentum (OAM), where m is known as topological charge (TC) and φ is azimuthal angle in the cylindrical coordinate system [1]. The application about OAM beams have been studied in many field, such as micromanipulations [2], optical pump [3], communications [4-5], detection [6]. In the past 20 years, researchers have proposed many methods to generate OAM beams, for instance spiral phase plates [7], computer-generated holograms [8], Q-plate [9], metasurface [10-13], coordinate transformation [14] and spiral pinhole plates [15-16]. The OAM beams made by the above methods are simple to manipulate a single OAM mode or simple superposition of several OAM modes, while, the OAM-based applications are not limited to a single mode in some occasions [17-19]. In 2019, Yang et al. [20] proposed a binary mask to generate photonic gears with a superposition of two OAM modes with opposite sign.

In this paper, we presented a NSP constructed by the inner and outer Fermat spiral pinholes (FSP) [21] arrays to generate the superposition of two different OAM modes, namely, bright ring lattice (BRL) [22], whose OAM modes can be controlled by adjusting the structure of NSP and the propagation distance. In addition, the expression for the rotational angle of BRL is derived. Numerical calculations are performed to analyze the influences of OAM modes of NSP and rotating NSP on the BRL. It is found that the BRL does not keep pace with the NSP, which provides a scheme for increasing the accuracy of micromanipulation [23].

2. Methods and results

2.1 The generation of BRL

FSP is selected as the basic unit of the diffractive plate. As shown in Figure 1(a), a single counterclockwise FSP is given. The azimuthal angle and radial coordinates of the nth pinhole of FSP are expressed as $\alpha_n = 2\pi n/M$, $r_n = (r_0 + l_a z\lambda\alpha_n/\pi)^{1/2}$ [21], where M is the numbers of pinholes, z is the propagation distance and r_0, l_a λ denote the initial radius, central topological and wavelength, respectively. The optical field generated by a single FSP includes wide OAM spectrum centered at central topological value l_a [20] and the complex amplitude of the field reads

* Corresponding authors. *E-mail address*: psliu@uestc.edu.cn (Pusheng Liu).

as

$$E_1(r,\varphi) = \sum_{l=-\infty}^{+\infty} A_l(r) exp(il\varphi) \quad (1)$$

$A_l(r)$ is amplitude corresponding to index l. These OAM modes can be refined to obtain some special modes by adding several identical FSPs equally spaced in the azimuthal angular domain to construct FSP arrays (FSPA). As shown in Figure 1(b), a FSPA containing 8 arms is given. Considering that the FSPA containing p arms is illuminated vertically by monochromatic plane wave (All the beams used in this paper are monochromatic plane waves, and it will not be described later), $\lambda = 532\text{nm}$, the complex amplitude of the diffractive field is

$$\mathrm{E}(r,\varphi) = \sum_{n=0}^{p-1} \sum_{l=-\infty}^{+\infty} A_l(r) exp(il\varphi) exp\left(in\frac{l2\pi}{p}\right) \quad (2)$$

The OAM mode m in $\mathrm{E}(r,\varphi)$ can be expressed as

$$\begin{aligned} E_m(r,\varphi) &= \sum_{n=0}^{p-1} A_m(r) exp(im\varphi) exp\left(in\frac{m2\pi}{p}\right) \\ &= A_m(r) e^{im\varphi} \frac{1-exp(i2m\pi)}{1-exp(i2m\pi/p)} \end{aligned} \quad (3)$$

From the equation (3), we know $E_m(r,\varphi) = pA_m(r)e^{im\varphi}$ for $m = np$ and $E_m(r,\varphi) = 0$ for $m \neq np$, where n is an integer. It means that some special OAM modes with a multiple of p remain and other modes vanish. Significantly, the proportion of central OAM mode l_a is absolutely dominant among these special modes [21].

In order to generate BRL, two different FSPA are nested together. As shown in Figure 2(a), the inner FSPA with 5 counterclockwise arms and the outer one with 10 counterclockwise arms are engraved on the plate. Figure 2(b) is the field-intensity pattern consisting of 5 bright petal-like structures at $\mathrm{z} = 1.00\text{m}$ and Figure 2(c) is the corresponding OAM spectrum [24]. It can be observed that the OAM spectrum centered at $l_{a,in} = 5$ and $l_{a,out} = 10$, where $l_{a,in}$ and $l_{a,out}$ are the central OAM modes of the inner and outer FSPA, respectively. The petal-like structure of the Figure 2 (b) is the superposition of two different OAM modes derived from the diffraction of the inner and outer FSPA, which is called BRL. We can produce different BRL by adjusting the structure of the NSP. Figure 2(d) represents another NSP consisting of 4 clockwise arms and 9 counterclockwise arms. It is obvious that the field-intensity pattern with 13 bright petals is depicted in the Figure 2(e) and the corresponding OAM spectrum on the Figure 2(f) centered at $l_{a,in} = -4$ and $l_{a,out} = 9$. It is known that from the Figure 2(a)-(f), the BRL with controllable OAM modes is realized, and the central OAM modes depend on the number of the inner and outer arms, where the positive and negative signs mean counterclockwise and clockwise arms, respectively.

The central mode of optical field generated by one single FSP varies with the increase of propagation distance z and the value of the central mode is inversely proportional to propagation distance [25]. As a result, different central modes can be obtained at different z by choosing the numbers of arms of FSPA, and variable BRL generated by NSP with increasing z is achieved. As shown in Figure 3 (a), the NSP contains 3 clockwise inner FSPA and 6 counterclockwise outer FSPA, Figure 3(b) is the intensity pattern of 18 bright petals at $\mathrm{z} = 1.00\text{m}$, where the central modes are $l_{a,in} = -6$ and $l_{a,out} = 12$, respectively. Modulating the propagation distance $\mathrm{z} = 2.00\text{m}$, the

field-intensity pattern of 9 bright petals with $l_{a,in} = -3$ and $l_{a,out} = 6$ is given in Figure 3(c).

2.2 The influences of rotating NSP on the BRL

Considering diffractive field of NSP, the complex amplitude generated by the inner and outer FSPA are denoted as $E_{in}(r,\varphi) = \mathrm{A}(r)\exp(il_{a,in}\varphi)$ and $E_{out}(r,\varphi) = A(r)exp(il_{a,out}\varphi)$, respectively, where we have ignored all the modes except the central modes. Without loss of generality, the outer FSPA are fixed and the inner one is rotated counterclockwise $\Delta\varphi_{in}$, and the complex amplitude of inner FSPA becomes $E'_{in}(r,\varphi) = A(r)exp[il_{a,in}(\varphi - \Delta\varphi_{in})]$. The intensity of superimposed field has the form

$$\mathrm{I} = |E'_{in} + E_{out}|^2 = 4|A(r)|^2\cos^2\left[\frac{(l_{a,in}-l_{a.out})\varphi - l_{a,in}\Delta\varphi_{in}}{2}\right] \quad (4)$$

It can be seen from equation (4) that the rotational angle of BRL is

$$\Delta\varphi = \frac{l_{a,in}\Delta\varphi_{in}}{l_{a,in}-l_{a,out}} \quad (5)$$

Equation (5) shows that $\Delta\varphi_{in}$ is determined simultaneously by $\Delta\varphi_{in}$, $l_{a,in}$ and $l_{a,out}$. It means that the rotational angle and direction of BRL are different from that of the inner FSPA.

Fig. 4(a) represents the images of rotating NSP and its corresponding diffractive patterns, where the NSP consists of 3 counterclockwise arms of the inner FSPA and 6 clockwise arms of the outer FSPA, and the central modes are $l_{a,in} = 3$ and $l_{a,out} = -6$, respectively. We can see from the Figure 4(a) that the inner arrays are rotated counterclockwise with an interval of $2\pi/5$ every time, while the BRL is rotated counterclockwise with an interval of $2\pi/15$. The direction of rotation of BRL is the same as that of the inner FSPA, but the rotational angle is smaller than the results of the inner FSPA. We can also construct a NSP to make behavior of the BRL completely different from the previous example. Figure 4(b) shows the diffractive image of NSP with 4 counterclockwise arms of the inner FSPA and 7 counterclockwise arms of the outer FSPA ($l_{a,in} = 4$ and $l_{a,out} = 7$), the inner FSPA of which rotates counterclockwise with an interval of $2\pi/5$, however, the BRL rotates clockwise with an interval of $8\pi/15$. It is worth nothing that we exchange a bigger rotational angle of FSPA for a smaller rotational angle of BRL to obtain an excellent accuracy of manipulations, and this effect can be used in the field of high-accuracy manipulations [22].

3. Conclusions

In this paper, we have designed NSP to generate produce BRL with controllable OAM modes by adjusting the structure of the NSP and propagation distance. Furthermore, the expression for the rotational angle of BRL is given, and the effects of rotating NSP on the BRL are studied in detailed. It is found that the BRL does not keep pace with the NSP, where the rotational direction and angle of the BRL are also related to the construction of NSP. The results of this work may provide a

scheme for increasing the accuracy of micromanipulation.

Acknowledgements
We thank Yuanjie Yang, Jiandong Wang, Yi Liu, Zhihong Zhang, Chaobin Lu for helpful discussion.

Author contributions
W.L., P.L. and Y.L. conceived the idea and theory. W.L. and P.L. wrote the manuscript.

Competing interests
The authors declare no competing interests

Reference

[1] Allen, L., Beijersbergen, M. W., Spreeuw, R. J. C. & Woerdman, J. P. Orbital angular momentum of light and the transformation of Laguerre-Gaussian laser modes. *Phys. Rev. A* **45,** 8185-8189; 10.1103/PhysRevA.45.8185 (1992).

[2] Rui, G., Wang, X. & Cui, Y. Manipulation of metallic nanoparticle with evanescent vortex Bessel beam. *Opt. Express* **23,** 25707; 10.1364/OE.23.025707 (2015).

[3] Leach, J., Mushfique, H., di Leonardo, R., Padgett, M. & Cooper, J. An optically driven pump for microfluidics. *Lab. Chip* **6,** 735-739; 10.1039/B601886F (2006).

[4] Wang, J. *et al.* Terabit free-space data transmission employing orbital angular momentum multiplexing. *Nat. Photonics* **6,** 488-496; 10.1038/nphoton.2012.138 (2012).

[5] Liu, L., Gao, Y. & Liu, X. High-dimensional vortex beam encoding/decoding for high-speed free-space optical communication. *Opt. Commun.* **452,** 40-47; 10.1016/j.optcom.2019.06.061 (2019).

[6] J.Lavery, M. P., Speirits, F. C., Barnett, S. M. & Padgett, M. J. Detection of a Spinning Object Using Light's Orbital Angular Momentum. *Science* **341,** 764-768; 10.1126/science.1239936 (2013).

[7] Beijersbergen, M. W., Coerwinkel, R. P. C., Kristensen, M. & Woerdman, j. p. Helical-wavefront laser beams produced with a spiral phaseplate. *Opt. Commun.* **112,** 321-327; 10.1016/0030-4018(94)90638-6 (1994).

[8] Heckenberg, N. R., McDuff, R., Smith, C. P. & White, A. G. Generation of optical phase singularities by computer-generated holograms. *Opt. Lett.* **17,** 221; 10.1364/OL.17.000221 (1992).

[9] Marrucci, L., Manzo, C. & Paparo, D. Optical spin-to-orbital angular momentum conversion in inhomogeneous anisotropic media. *Phys. Rev Lett.* **96,** 163905; 10.1103/PhysRevLett.96.163905 (2006).

[10] Zheng, Q. *et al.* Efficient orbital angular momentum vortex beam generation by generalized coding metasurface. *Appl. Phys. A* **125,** 1900594; 10.1007/s00339-018-2373-z (2019).

[11] Zhao, Z., Wang, J., Li, S. H. & Willner, A. E. Metamaterials-based broadband generation of orbital angular momentum carrying vector beams. *Opt. Lett.* **38,** 932-934; 10.1364/OL.38.000932 (2013).

[12] Yu, N. *et al.* Light propagation with phase discontinuities: generalized laws of reflection and refraction. *Science* **334,** 333-337; 10.1126/science.1210713 (2011).

[13] Liu, X., Deng, J., Jin, M., Tang, Y. & Li, G. Cassegrain metasurface for generation of orbital angular momentum of light. *Appl. Phys. Lett.* **115,** 221102; 10.1063/1.5127007 (2019).

[14] Wen, Y., Chremmos, I., Chen, Y., Zhang, Y. & Yu, S. Arbitrary Multiplication and Division of the Orbital Angular Momentum of Light. *Phys Rev Lett.* **124,** 213901; 10.1103/PhysRevLett.124.213901 (2020).

[15] Li, Z. *et al.* Generation of high-order optical vortices with asymmetrical pinhole plates under plane wave illumination. *Opt Express* **21,** 15755-15764; 10.1364/OE.21.015755 (2013).

[16] Ma, L. *et al.* Spatiotemporal evolutions of ultrashort vortex pulses generated by spiral multi-pinhole plate. *Opt Express* **25,** 29864-29873; 10.1364/OE.25.029864 (2017).

[17] Wei, D. *et al.* Laguerre-Gaussian transform for rotating image processing. *Opt Express* **28,** 26898-26907; 10.1364/OE.403521 (2020).

[18] Li, F. *et al.* Optical images rotation and reflection with engineered orbital angular momentum spectrum. *Appl. Phys. Lett.* **113,** 161109; 10.1063/1.5043229 (2018)

[19] Zhang, W. & Chen, L. Encoding and decoding of digital spiral imaging based on bidirectional transformation of light's spatial eigenmodes. *Opt Lett.* **41,** 2843-2846; 10.1364/OL.41.002843 (2016).
[20] Yang, Y. *et al.* Manipulation of Orbital-Angular-Momentum Spectrum Using Pinhole Plates. *Phys. Rev. Appl.* **12,** 064007; 10.1103/PhysRevApplied.12.064007 (2019).
[21] Yang, Y., Thirunavukkarasu, G., Babiker, M. & Yuan, J. Orbital-Angular-Momentum Mode Selection by Rotationally Symmetric Superposition of Chiral States with Application to Electron Vortex Beams. *Phys Rev Lett.* **119,** 094802; 10.1103/PhysRevLett.119.094802 (2017).
[22] Franke-Arnold, S. *et al.* Optical ferris wheel for ultracold atoms. *Opt Express* **15,** 8619-8625; 10.1364/OE.15.008619 (2007).
[23] Gecevicius, M., Drevinskas, R., Beresna, M. & Kazansky, P. G. Single beam optical vortex tweezers with tunable orbital angular momentum. *Appl. Phys. Lett.* **104,** 231110; 10.1063/1.4882418 (2014).
[24] Lluis, T., Juan, T. & Silvia, C. Digital spiral imaging. *Opt Express* **13,** 873-881; 10.1364/OPEX.13.000873 (2005).
[25] Yang, Y. *et al.* Anomalous Bessel vortex beam: modulating orbital angular momentum with propagation. *Nanophotonics* **7,** 677-682; 10.1515/nanoph-2017-0078 (2018).

Figure captions

Figure 1. The construction of FSP arrays.
(**a**) a single FSP. (**b**) FSPA with 8 arms equally spaced in the azimuthal angular domain

Figure 2. Simulated results for generating BRL.
(**a**)-(**c**) NSP with 5 counterclockwise arms of the inner FSPA and 10 counterclockwise arms of the outer FSPA; the corresponding initial radii of two FSPA r_0 are 1.5mm and 3mm, respectively. (**d**)-(**f**) NSP with 4 clockwise arms of the inner FSPA and 9 counterclockwise arms of the outer FSPA, the initial radii r_0 are 1.3mm and 3mm, respectively. The corresponding field-intensity patterns (**b**) and (**e**), and OAM spectrum (**c**) and (**f**) at $z = 1.00$m.

Figure 3. The central OAM modes of the BRL vary with the propagation distance z
(**a**) NSP with 3 clockwise inner arms and 6 counterclockwise arms; the corresponding initial radii of two FSPA r_0 are 1.5mm and 3mm, respectively. the intensity patterns at $z = 1.00m$ (**b**) and $z = 2.00m$ (**c**).

Figure 4. The influences of rotating NSP on the BRL
(**a**) NSP with 3 counterclockwise inner arms and 6 clockwise outer arms. (**b**) NSP with 4 counterclockwise inner arms and 7 counterclockwise outer arms, the top part of (**a**) and (**b**) show the rotating of the NSP, the corresponding bottom of the part are the rotating of the BRL. In order to observe their rotational angle, a spiral arm of the NSP was painted red and a petal of the BRL was marked in blue. The white rotating arrows on the left side of the figure indicate the rotational direction of the NSP (or BRL) from left to right. The number of each picture represent the rotation angle of the NSP (or BRL).

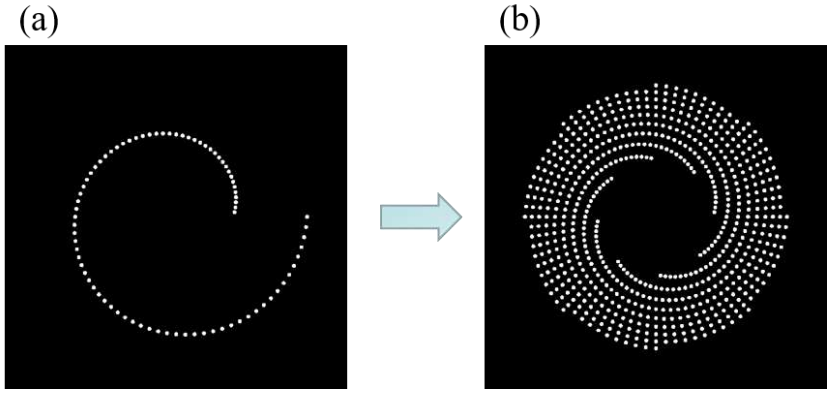

Figure 1. The construction of FSP arrays.
(**a**) a single FSP. (**b**) FSPA with 8 arms equally spaced in the azimuthal angular domain

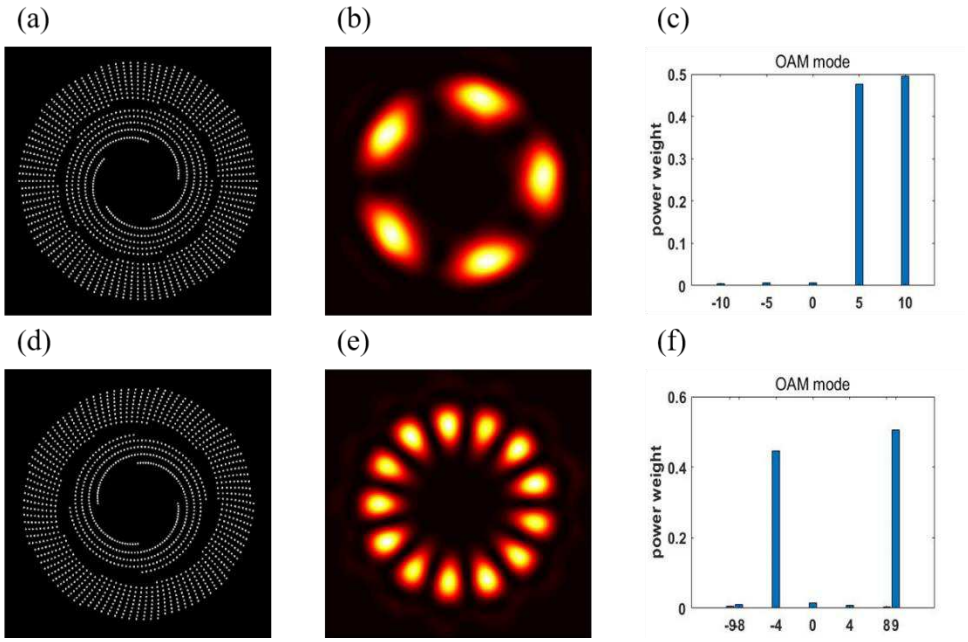

Figure 2. Simulated results for generating BRL.

(**a**)-(**c**) NSP with 5 counterclockwise arms of the inner FSPA and 10 counterclockwise arms of the outer FSPA; the corresponding initial radii of two FSPA r_0 are 1.5mm and 3mm, respectively. (**d**)-(**f**) NSP with 4 clockwise arms of the inner FSPA and 9 counterclockwise arms of the outer FSPA, the initial radii r_0 are 1.3mm and 3mm, respectively. The corresponding field-intensity patterns (**b**) and (**e**), and OAM spectrum (**c**) and (**f**) at $z = 1.00$m.

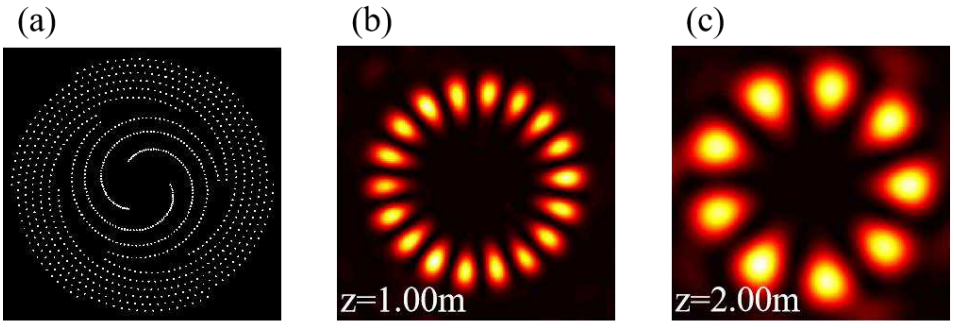

Figure 3. The central OAM modes of the BRL vary with the propagation distance z

(**a**) NSP with 3 clockwise inner arms and 6 counterclockwise arms; the corresponding initial radii of two FSPA r_0 are 1.5mm and 3mm, respectively. the intensity patterns at $z = 1.00m$ (**b**) and $z = 2.00m$ (**c**).

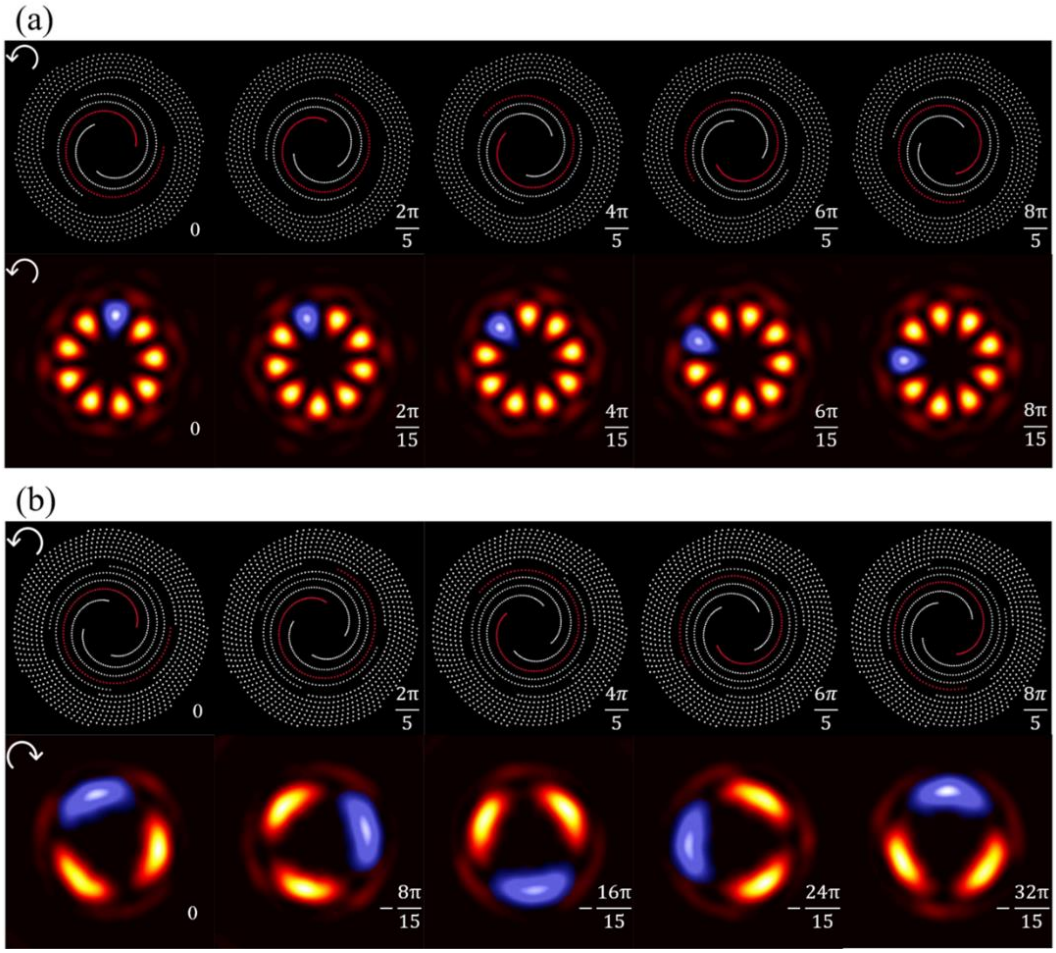

Figure 4. The influences of rotating NSP on the BRL

(**a**) NSP with 3 counterclockwise inner arms and 6 clockwise outer arms. (**b**) NSP with 4 counterclockwise inner arms and 7 counterclockwise outer arms, the top part of (**a**) and (**b**) show the rotating of the NSP, the corresponding bottom of the part are the rotating of the BRL. In order to observe their rotational angle, a spiral arm of the NSP was painted red and a petal of the BRL was marked in blue. The white rotating arrows on the left side of the figure indicate the rotational direction of the NSP (or BRL) from left to right. The number of each picture represent the rotation angle of the NSP (or BRL).